ISSN: 0067-2904

Preparation Dye- Sensitized Solar Cells Based on ZnO Films and Shami Berries Natural Dye

Ola Shaher Amer , Ibrahim Alghoraibi*
Physics Department, Faculty of Science, Damascus University, Damascus, Syria.

Received: 2/6/2023 Accepted: 24/3/2024 Published: 30/3/2025

Abstract

The photoelectrode of the dye-sensitized solar cells was fabricated by sensitizing ZnO with a natural extract of Shami berries with different solvents. The working electrode of ZnO nanoparticles was synthesized using the sol-gel and dip-coating method and deposited onto ITO substrates using zinc acetate dihydrate as a precursor. The study investigated the effect of solvent type (methanol and ethanol), substrate withdrawal speed (1mm/s and 5mm/s), and catalyst agent (Triethanolamine (TEA) and Monoethanolamine (MEA)) on photoconversion in the dye-sensitized solar cell. An atomic force microscope examined the nanostructure of the prepared film, indicating nanoparticle sizes in the range from 48 to 105 nm. The optical properties analyzed with a UV-Vis spectrophotometer (wavelength: 300-800 nm) showed a band gap energy of 3.26 eV for the ZnO thin films sensitized with methanol as solvent, withdrawal speed of 1mm/s and TEA as the catalyst agent. The band gap energy for Shami berries extract with acidified ethanol as the solvent was found to be 1.7eV. Cyclic voltammetry estimated the energy levels of the dye's highest occupied molecular orbital (HOMO) and lowest unoccupied molecular orbital (LUMO) at -5.2 eV and -3.5 eV, respectively. Additionally, the study evaluated the efficiency of dye-sensitized solar cells under optimal experimental conditions. The DSSC utilizing Shami berries extract with acidified ethanol had the highest photoconversion efficiency (η) of 0.79%.

Key Words: Atomic force microscopy (AFM), Catalyst agent, Dye-sensitized solar cells, Energy dispersive X-ray spectroscopy (EDX), Natural dyes, Nanoparticles of zinc oxide (ZnO-NPs), Sol-Gel method, The Cyclic voltammetry (C-V).

تحضير خلايا شمسية صباغية باستخدام أوكسيد الزنك النانوي وصباغ التوت الشامي الطبيعي

علا شاهر عامر,ابراهيم الغريبي *

قسم الفيزياء، كلية العلوم، جامعة دمشق، دمشق، سورية

الخلاصة:

تم تحضير الالكترود الضوئي للخلايا الشمسية الصباغية من أوكسيد الزنك وصباغ التوت الشامي الطبيعي المستخلص بمحلات مختلفة. حُضرت حبيبات أوكسيد الزنك بطريقة السول الجل المعززة بالغمس على ركائز زجاجية ناقلة كهربائياً (ITO) باستخدام محلول خلات الزنك كمصدر لأيونات الزنك. تناولت الدراسة تأثير نوع المذيب وسرعة سحب الركائز ونوع العامل المحفز على غشاء أوكسيد الزنك. وصِّفت الأغشية المحضرة بنيوياً باستخدام مجهر القوة الذرية (AFM) حيث بيّنت الدراسة تشكل حبيبات نانوية كروية الشكل أبعادها حوالي 48–105nm، تم التوصيف الضوئي باستخدام UV–VIS في مجال الطول

*Email: ola.amer@damascusuniversity.edu.sy

الموجي (300–800nm). قُدرت فجوة الطاقة لغشاء أوكسيد الزنك المحضر بالشروط المثلى 3.26 eV وذلك باستخدام الميثانول كمحل و 1mm/s سرعة لسحب الركائز و TEA كعامل محفز. كما قُدرت فجوة الطاقة للصباغ المستخلص باستخدام الإيثانول المُحمض 1.7eV. أظهرت الدراسة الكهركيميائية باستخدام تقانة السايكلوفولطومتري الحلقي لمحاليل الصباغ المحضرة ظهور قمة الأكسدة والارجاع بشكل واضح باستخدام الماء المحمض، حيث كانت قيمة أعلى مدار جزئي مشغول HOMO وأدنى مدار جزئي غير مشغول LUMO 3.5 eV , – 5.3 eV – على الترتيب. تهدف الدراسة إلى تقييم كفاءة الخلايا الشمسية الصباغية باستخدام الشروط التجريبية المثلى. الخلية الشمسية الصباغية المحضرة باستخدام التوت الشامي المستخلص بالإيثانول المحمض أظهرت أعلى قيمة للمردود وصل إلى 0.79%.

Introduction:

Zinc oxide (ZnO) has a wide band gap of 3.2-3.37 eV at room temperature [1] and high electron mobility of ~ 115 - 155 $cm^2.V^{-1}.s^{-1}$ [2]. In addition, it is possible to control the range of absorbed wavelength of the sunlight spectrum by controlling the ZnO nanoparticle sizes and experiment conditions [3]. ZnO thin film has been popularly used in fields of piezoelectric devices [4], solar cell electrodes [5], photocatalysis [6], gas sensors [7] and optoelectronics [8]. ZnONPs thin film can be found in different structures, such as nanoparticles [9], nanowires [10], nanofibers [11], nanorods [12] and nanoflowers [13]. For solar cell applications, ZnO nanostructures are synthesized using various methods, such as spray pyrolysis [14], chemical bath deposition [15], pulsed laser deposition [16], hydrothermal method [17] , electrochemical deposition [18] and sol-gel technique [19] have been used as antireflective layers. The sol-gel dip-coating technique stands out as a widely used method for depositing thin films. This approach eliminates the necessity for high temperatures or highly pure chemical materials, making it a convenient, cost-effective, and easily manageable method for applying metal oxide films on large surfaces [20]. For this study, the sol-gel dip coating was chosen for the deposition of ZnO thin films on Indium-doped Tin Oxide (ITO) substrates.

In recent years, dye-sensitized solar cells have attracted much attention due to their low cost and eco-friendliness compared to other types of solar cells. Dye-sensitized solar cells (DSSC) are classified as the third generation of solar cells and one of the strongest contenders for perovskites [21]. Figure (1) shows a schematic diagram illustrating the electron transfer mechanism of dye-sensitized solar cells [1], where high-quality nanocrystalline material plays an essential role in electron injection and transport and the performance of the DSSC.

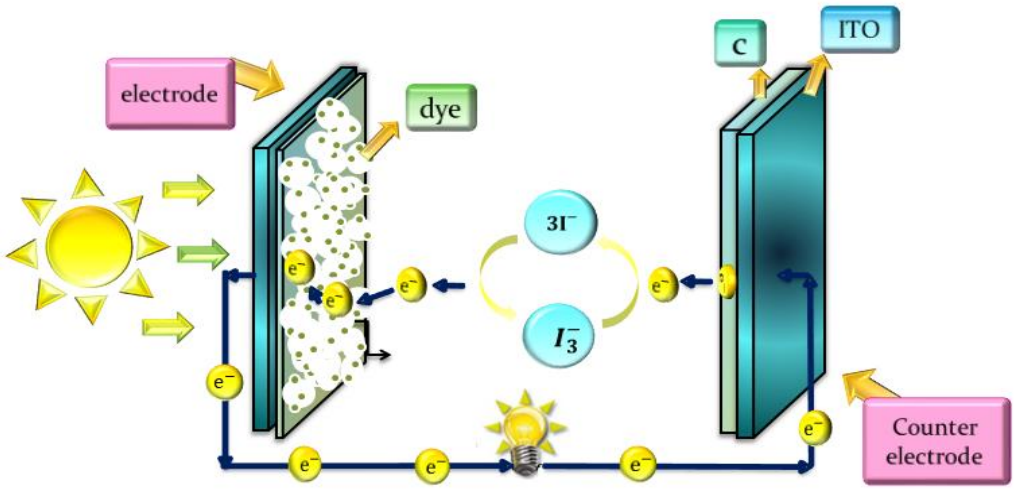

Figure 1: The schematic electron transfer mechanism of dye sensitized solar cells.

The basic idea is the conversion of photons into current [22]. This includes four main steps: light absorption, electron injection, transportation process, and collection of current, as shown in Figure (2):

(1) Upon absorbing a photon, electrons get excited from the ground state (S) to an excited state(S^*) of the dye, where most absorption occurs in the dye. (2) The excited electrons injected into the conduction band of ZnO particles existing under the excited state of the dye getting oxidized. (3) The injected electrons are transported across ZnO particles and diffusing through the external circuit to reach the counter electrode. (4) The counter electrode electrons reduce I^{-3} ions to I^-; i.e, the ground state of the dye takes electrons from I^- ion redox mediator, and I^- gets oxidized to I^{-3} (oxidized state). (5) The oxidized mediator (I^{-3}) diffuses to the counter electrode and reduces to I−.

- $S + hv \rightarrow S^*$
- $S^* \rightarrow S + e^-$ (to ZnO)
- $S^* + e^- \rightarrow S$
- $I^{-3} + 2e^- \rightarrow 3\,I^-$

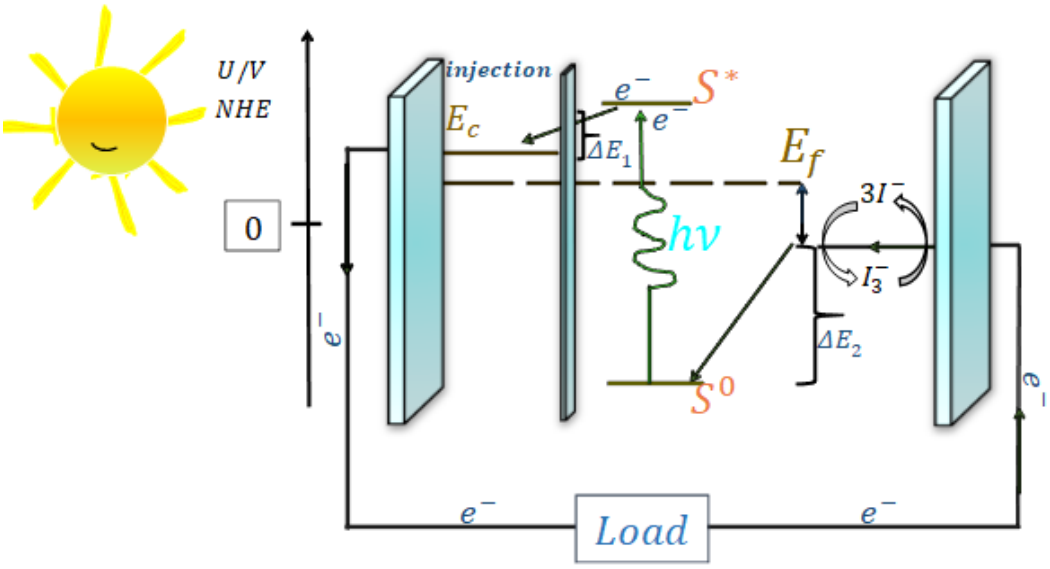

Figure 2: Working principle of the DSSC.

In this paper, Shami berries were used as the dye sensitizer. It was prepared with different solvents, and its effect on the performance of DSSCs was studied. The effect of various parameters, such as the type of solvent, substrate withdrawal speed and catalyst agent type, on the structural, morphological and optical properties of ZnO was investigated. A sight and understanding of these parameters features and their influence on DSSC performance are provided.

Experimental:

1. Photoelectrode (the working electrode) Preparation:

1.1 Preparation of ZnO thin films: ZnO thin films were deposited by the sol-gel dip coating method on transparent conductive ITO/glass with a resistivity of 10–12Ω.cm, a transmittance > 80% and an area of $2cm^2$. Zinc acetate dihydrate ($Zn(CH_3COO)_2.2H_2O$) was used as a source of zinc ions. To deposit ZnO thin films onto ITO/glass substrate, 2.2g of zinc acetate dihydrate was mixed with 50ml of different solvent solutions (methanol and ethanol) and magnetically stirred at 25^0C for 50 min to get homogeneous mixtures. Two catalyst agents were used: triethanolamine (TEA) and monoethanolamine (MEA). 2ml of triethanolamine (TEA) and monoethanolamine (MEA) were gradually added to the solutions until they

became colorless. Cleaned ITO substrates were vertically immersed five times into each of the prepared solutions, using a home-made dip coating apparatus, with various withdrawal speeds of 1mm/s and 5mm/s to obtain a thin film of approximately 100nm thickness, as measured by the gravimetric method. The samples withdrawn upward were rinsed ultrasonically in distilled water for 10 min to remove non-adherent ZnO layer; then, the samples were dried in an oven at room temperature and followed by thermal treatment at 500^0C for an hour [23].

2.1 Preparation of Natural Dye Sensitizer:

Anthocyanin-based natural dye was isolated from Shami berries. 300g of the natural fruit was smashed with a milling machine. The extract was prepared without a solvent and with different solvents: ethanol and acidified ethanol (80% ethanol, 1% HCl) (100ml of each solvent). The residuals were filtered using Whatman No. 1 filter. Mixtures of the above three dye solutions were kept in dark bottles to be used later.

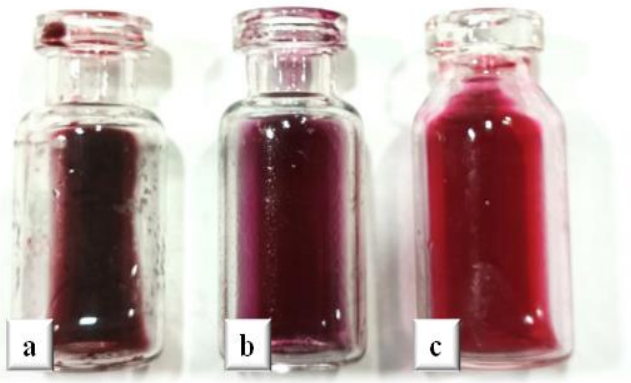

Figure 3: Image of the prepared natural dye with different solvent a) without solvent, b) with ethanol, c) with acidified ethanol.

3.1 ZnO photoelectrode(the working electrode) preparation:

The coloring of the ZnO/ITO/glass electrodes with the dye (see Figure (4)) were carried out by soaking them in the dye solutions. The electrodes were immersed in the dye solutions while still hot at 70^0Cfor 24 hrs. After that, the dye-coated films were washed with ethanol and stored in the dark in an air-tight case until cell assembly.

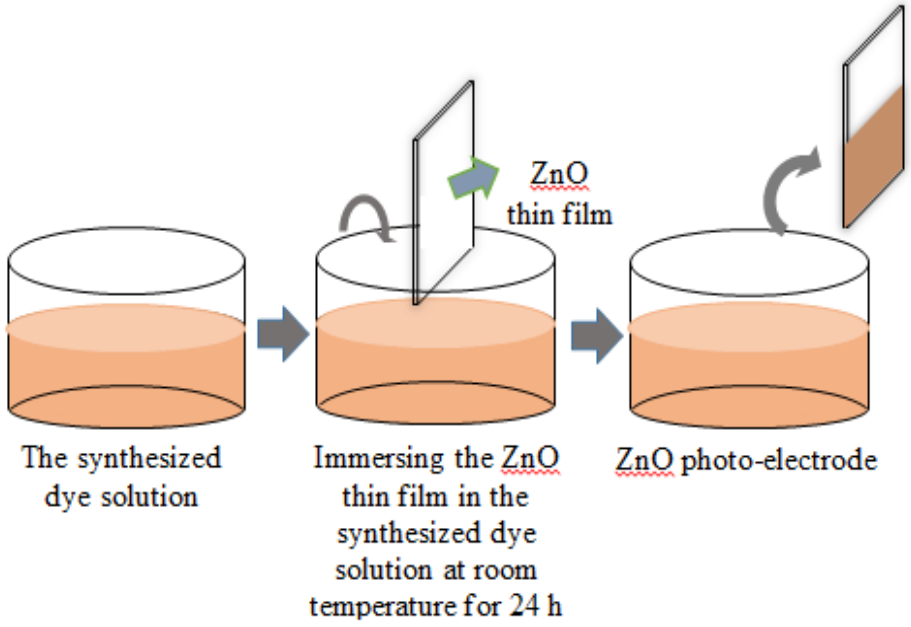

Figure 4: The process of ZnO photoelectrode preparation method.

2. Electrolyte and counter electrode preparation:

The electrolyte solution was prepared by thoroughly mixing 0.83g of KI and 0.126g of I_2 in 10ml methoxyacetonitrile for 15min, the electrolyte solution was kept in a black container to be used later. A carbon soot counter electrode was prepared by exposing ITO glass to candlelight for 2min.

3. Assembling a complete dye solar cell:

The electrodes were arranged to form a standard sandwich-type cell, positioning the photoelectrode facing upwards and aligning it with the conductive side of the carbon counter electrode. This arrangement allowed the ZnO/ITO/glass electrode with the dye to be covered by the carbon counter electrode. A few drops of the electrolyte were injected in between the two electrodes, and cables were connected to the terminals on the sides of the cell to facilitate data collection. As shown in Figure (5), the assembly of the dye-sensitized solar cell was finalized using binder clips to ensure proper connectivity between the two slides.

Figure 5: A picture of the prepared dye-sensitized solar cell.

Results and Discussion:

Topographical properties were assessed in this study using atomic force microscope ((AFM, Nanosurf easyScan2, Switzerland, Tap190 Al-G, NanoSensors™)) to obtain surface information and determine the influence of the solvent solutions (methanol or ethanol), the

substrate withdrawal speed (1 and 5 mm/s), and the catalyst agent (TEA or MEA) on the morphology and quality of the as-deposited ZnO films. A 2µm x 2µm AFM images of the prepared films are presented, as shown in Figure (6). The results confirm that the ZnO thin films have uniform morphology with complete coverage of the substrate surface. The AFM images and size distribution for ZnO thin films using the two solvents, methanol and ethanol, are shown in Figures (6a and 7b), keeping the other parameters constant at a withdrawal speed of 1mm/s and TEA as the catalyst agent. The mean diameter of ZnO nanoparticles was 48 nm and 64 nm for methanol and ethanol, respectively [24].

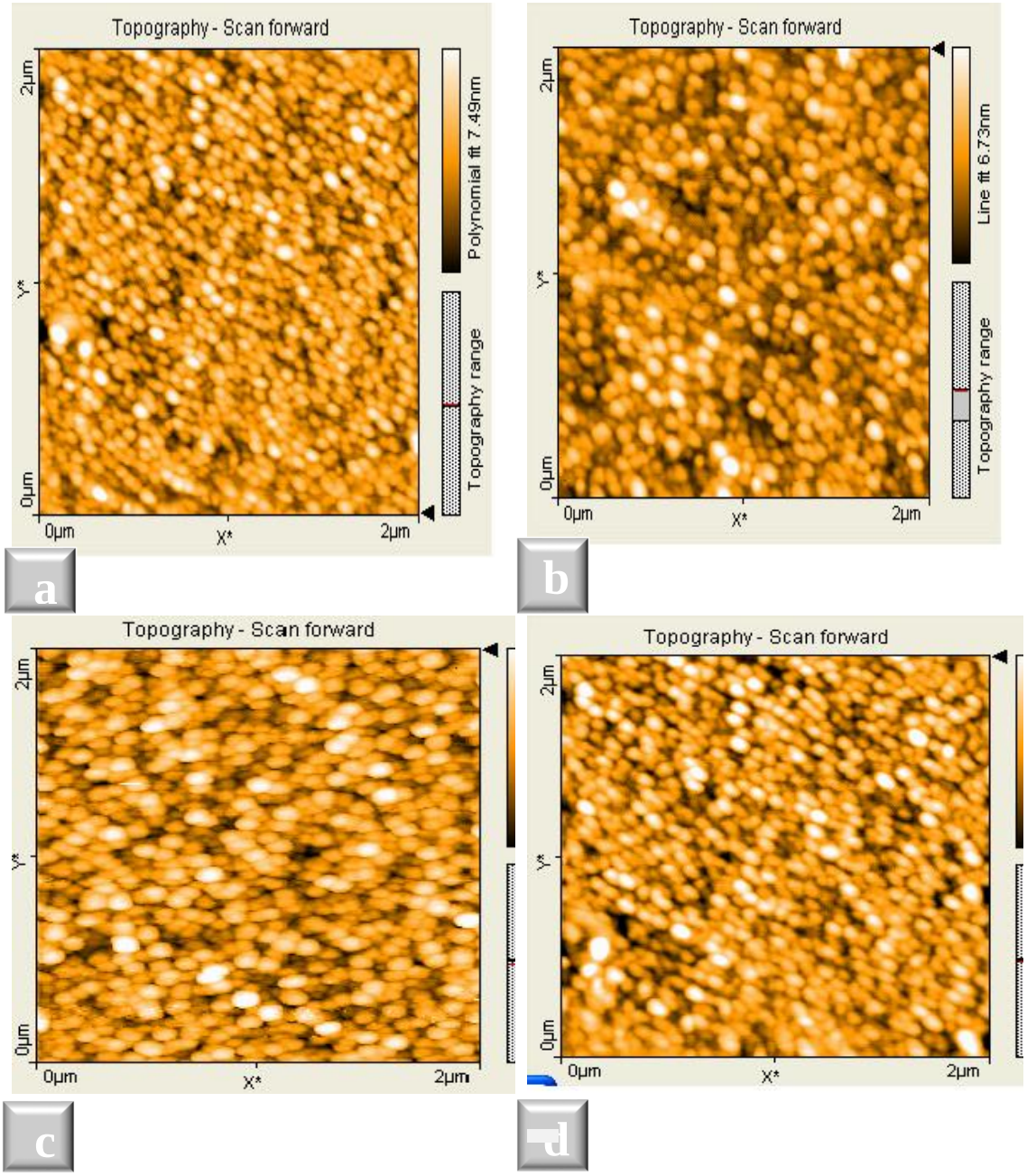

Figure 6: The AFM surface ($2\mu m \times 2\mu m$) images of the ZnO thin films using:
a) methanol, withdrawal speed of 1mm/s and TEA, b) ethanol, withdrawal speed of 1mm/s and TEA c) methanol, withdrawal speed of 5mm/s, and TEA, d) methanol, withdrawal speed of 1mm/s, and MEA

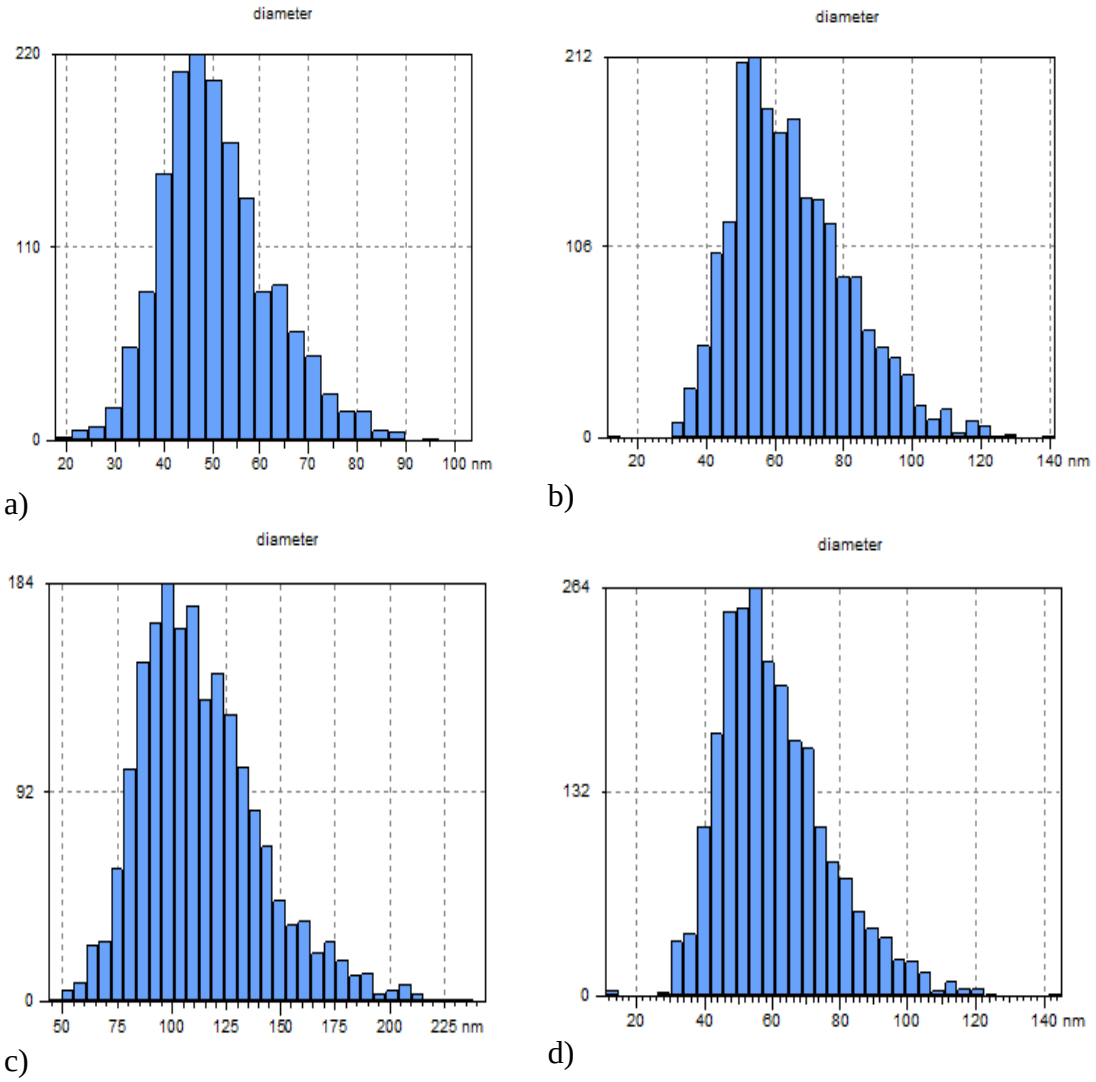

Figure 7: The nanoparticles size of the ZnO thin film using: a) methanol, withdrawal speed of 1mm/s and TEA, b) ethanol, withdrawal speed of 1mm/s and TEA c) methanol, withdrawal speed of 5mm/s, and TEA, d) methanol, withdrawal speed of 1mm/s, MEA.

Comparing the AFM images at different withdrawal speeds of 1mm/s and 5mm/s utilizing methanol as the solvent and TEA as the catalyst, it was observed that the lower speed was the most suitable to form ZnONPs with small diameters, narrow size distributions, and uniform spherical shapes. Reducing the withdrawal speeds from 5mm/s to 1mm/s decreased the average diameter by 54%. The ZnO thin films prepared using MEA as the catalyst agent (see Figure 6-d) exhibit a uniform distribution with an average diameter ($\bar{R}$=56 nm) and a root mean square (Sq=1.55 nm), as shown in Fig (7) and Table (1).

Table 1: The average diameter and root mean square of ZnO nanoparticles film under various parameters.

	Using methanol, with withdrawal speed of 1mm/s and TEA	Using ethanol, withdrawal speed of 1mm/s and TEA	Methanol, withdrawal speed of 5mm/s, and TEA	Methanol, withdrawal speed of 1mm/s, and MEA
average diameter $\bar{R}(nm)$	48	64	105	56
root mean square $S_q(nm)$	1.10	1.20	2.25	1.55

Its surface composition was analyzed by energy dispersive X-ray spectroscopy (EDX). The EDX spectra shown in Figure (8) indicate that oxygen (O), zinc (Zn), calcium (Ca), and silicon (Si) were detected as elements. The weight and atomic percentage concentrations obtained by EDX analysis for as-deposited films are summarized in the insets table in the figure. The results illustrated a good quality ZnO thin film without common impurities. The observed elemental peaks corroborate the presence of Zn and O in the prepared thin film. Additionally, peaks of Na and Si atoms were detected, which may originate from the ITO/glass substrate.

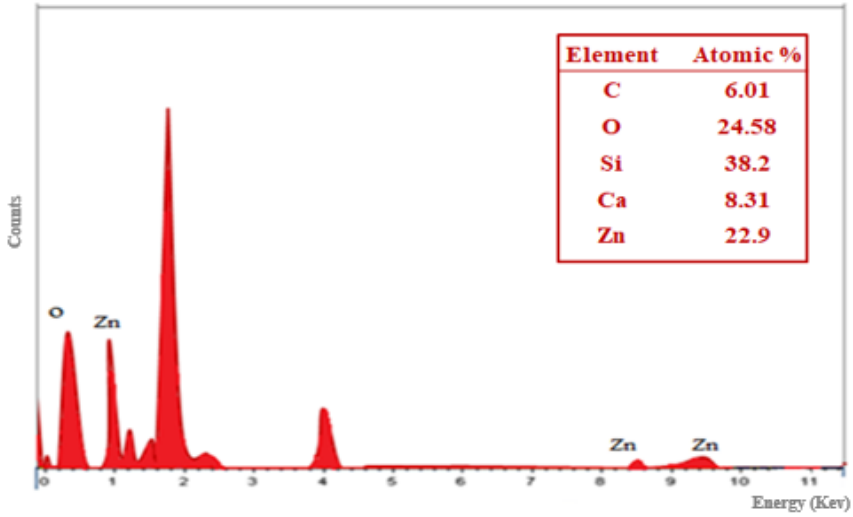

Figure 8: EDX spectrum of the optimized ZnO thin film.

The optical properties of the prepared ZnO thin films were assessed by UV-Vis spectra, as shown in Figure (9). The UV absorption spectra appeared between 360 to 400 nm wavelength.

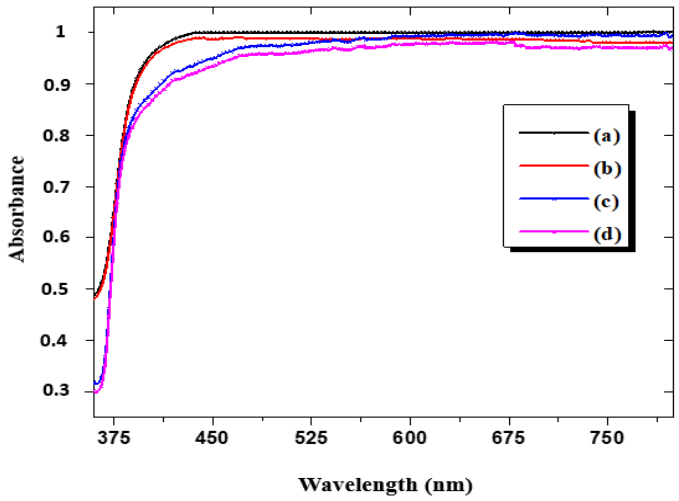

Figure 9: Variation of absorbance vs wavelength of ZnO thin film for different parameters using:
a) methanol, withdrawal speed of 1mm/s and TEA, b) ethanol, withdrawal speed of 1mm/s and TEA,
c) methanol, withdrawal speed of 5mm/s, and TEA, d) methanol, withdrawal speed of 1mm/s, and MEA

It is observed that the absorbance values of the prepared films undergo slight variations, which can be attributed to experimental conditions associated with changes in the dimensions of zinc oxide nanoparticles.

The band gap energy (E_g) of a semiconductor can be derived from Tauc formula as follows: $\alpha h\nu = A(h\nu - E_g)^n$, where α is the absorption coefficient, hν is the energy of the incident photons, A is a constant proportional to amorphosity, h is Planck's constant, ν is photon frequency, n is ½ for allowed direct energy gap and E_g is optical band gap energy. figure (10) shows the graphs of $(\alpha h\nu)^2$ vs. energy photon. The optical band gap energies of the films were estimated from the intercept of the extrapolated straight-line portion of the spectrum with the hν -axis at $(\alpha h\nu)^2=0$ [25].

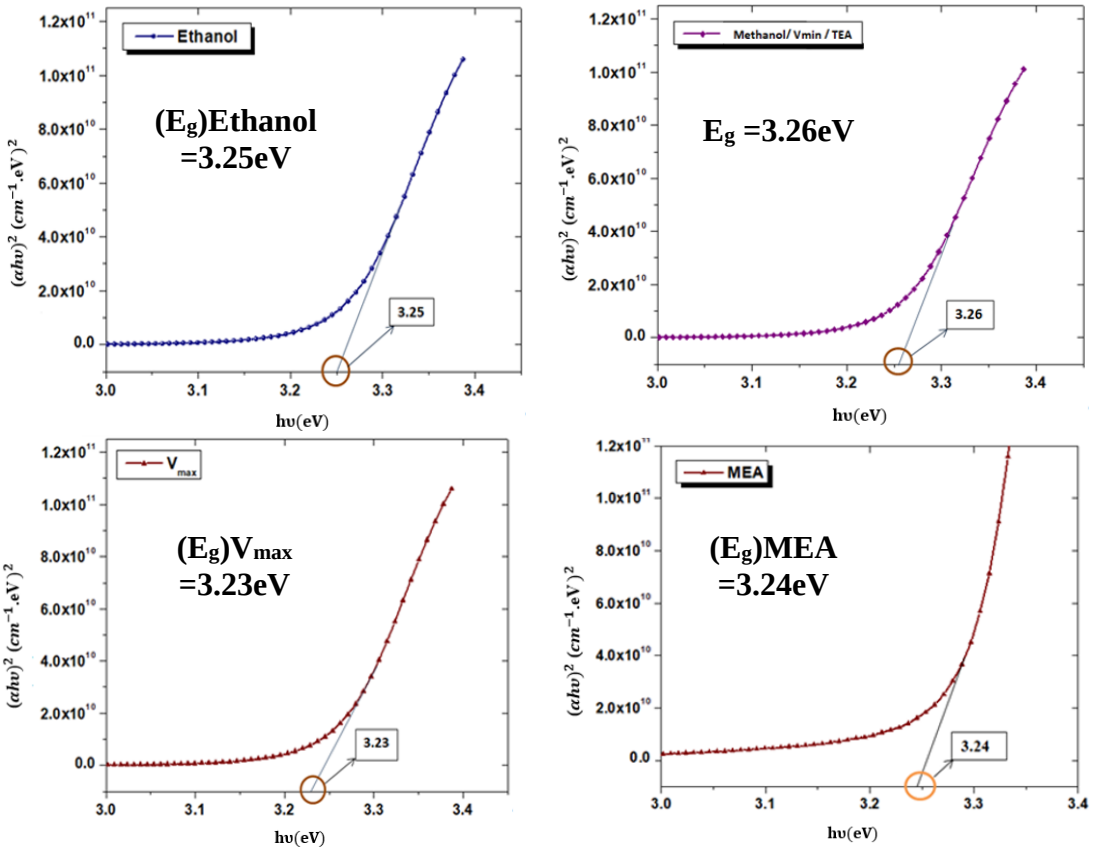

Figure 10: plot $(\alpha h\nu)^2$ against (hν) energy photon of ZnO deposited at various parameters using:
a) methanol, withdrawal speed of 1mm/s and TEA, b) ethanol, withdrawal speed of 1mm/s and TEA,
c) methanol, withdrawal speed of 5mm/s, and TEA, d) methanol, withdrawal speed of 1mm/s, and MEA

The band gap was evaluated for ZnO films, as shown in

Table 2: Table(2)- The band gap value of ZnO nanoparticles film under various parameters.

	Using methanol, with withdrawal speed of 1mm/s and TEA	Using ethanol, withdrawal speed of 1mm/s and TEA	Methanol, withdrawal speed of 5mm/s, and TEA	Methanol, withdrawal speed of 1mm/s, and MEA
The band gap value	3.26	3.25	3.23	3.24

The optimized ZnO thin film showed a band gap energy of 3.26 eV. The values were close to the standard ZnO band gap energy of ~3.35 eV at room temperature [26].
Figure (11) illustrates the absorption spectra of Shami-berries extracts without solvent, with ethanol and with acidified ethanol solvents. The absorption peaks were at approximately 470 nm, 510 nm and 560 nm, respectively. The difference in absorption characteristics was attributed to the presence of different colors of extract due to type of the solvent used. The highest absorption was noted when using acidified ethanol, which was attributed to the heightened solubility of the Shami-berry extract in this solvent and the greater amount of dye extracted.

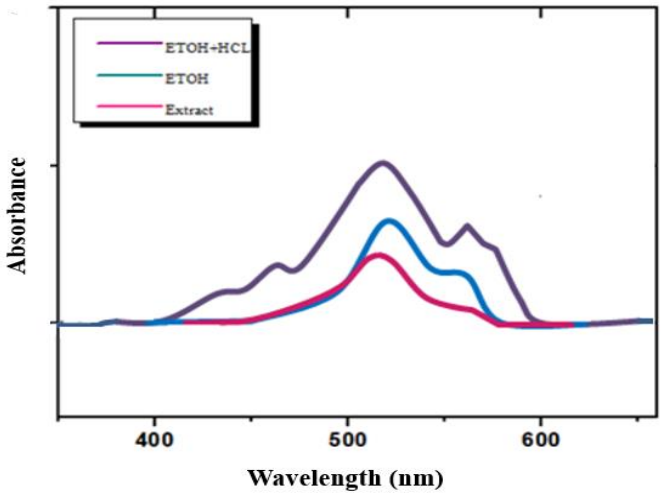

Figure 11: Absorbance spectra of Shami-berries extract without using solvent, with ethanol and with acidified ethanol.

Cyclic voltammetry (C-V) is one of the most useful methods for estimating the energy levels of the dye. The band value was obtained by Eqs (1), (2) and (3) [27]:

$$E_{HOMO} = -e\left[E_{Oxidation}^{Onset} + 4.4\right] \quad (1)$$

$$E_{LUMO} = -e\left[E_{\text{Reduction}}^{Onset} + 4.4\right] \quad (2)$$

$$E_g = E_{LUMO} - E_{HOMO} \quad (3)$$

Where: E_{HOMO} is the energy level of the highest occupied molecular orbital (HOMO), E_{LUMO} is the energy level of the lowest unoccupied molecular orbital (LUMO), $E_{Oxidation}^{Onset}$ and $E_{Reduction}^{Onset}$ are the values of the oxidation and reduction energy, respectively, and the value 4.4 is the adjustment factor. The C-V characterization using platinum and potassium chloride for the counter electrode and the reference electrode, respectively. The measurements were executed in a dark room at 25^0C with a scan rate of 50 mV/s and step potential of 0.01V. The

$E_{Oxidation}$ and $E_{Reduction}$ were evaluated using the C-V plots shown in Figure (12). The results revealed that no apparent oxidation and reduction peaks appeared for the extract without solvent and with ethanol solvent, as noted in Figure (12a,12b). On the other hand, for Shami-berries extract with acidified ethanol the values of the E_{HOMO}, E_{LUMO} and E_g were -5.2eV, -3.5eV and 1.7eV, respectively, as seen in Figure (12c).

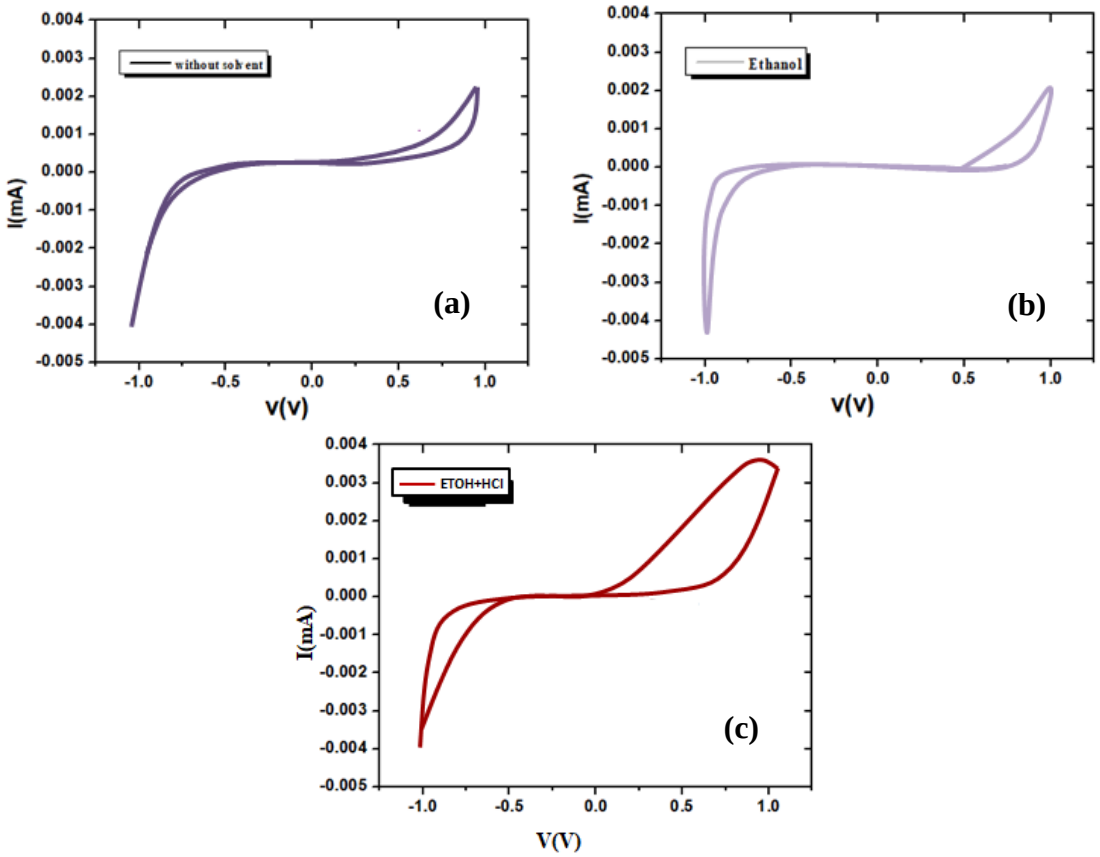

Figure 12: Cyclic voltammetry curve of Shami berries extracts a) without solvent, b) with ethanol solvent, c) acidified ethanol solvent

It is noteworthy that the calculated values for the Shami berries dye with acidified ethanol solvent are consistent with the fundamental principle of DSSC due to the E_{HOMO} level of the dye being lower than the redox level of electrolyte. The E_{LUMO} is sufficiently higher than the conduction band of ZnO, as shown in Figure (13)[28].

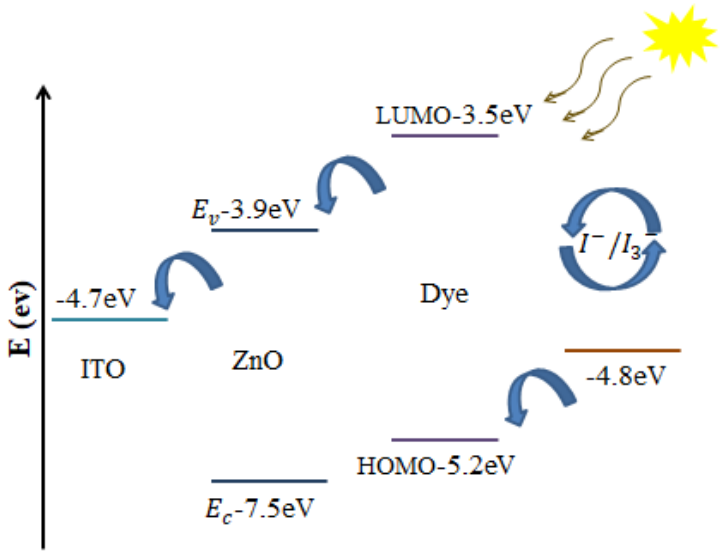

Figure 13: Energy levels diagram in ZnO/dye.

Evaluation of Dye-Sensitized Solar Cell Performance:

The performance of a dye-sensitized solar cell can be studied by evaluating the open circuit voltage (V_{oc}), short circuit current (I_{sc}), overall efficiency (η %), and fill factor (FF). The efficiency (η) of the DSSC can be estimated using the formula $\eta=P_{max}/P_{in}$, where P_{max} and P_{in} represent the maximum output power and the input power, respectively[29]. Moreover, The ratio of ($I_{max} \times V_{max}$) to the ($I_{sc} \times V_{oc}$) gives FF[30]. Figure (14) displays the current-voltage (I-V) characteristics of the DSSCs.

The conversion efficiency (η) of the cell with the Shami berries extract without solvent was 0.15% with a short circuit current of 0.88mA, an open circuit voltage of 119mV, and a fill factor of 0.68, while the conversion efficiency (η) using Shami berries with ethanol was 0.35% with a short circuit current of 1.04 mA, an open circuit voltage of 250mV, and a fill factor of 0.75. Whereas the DSSC utilizing Shami berries extract with acidified ethanol had the highest conversion efficiency (η) of 0.79% with a short circuit current of 1.29mA, an open circuit voltage of 360mV and a fill factor of 0.80. It is noted that the solar cells prepared using Shami berries extract with acidified ethanol as the solvent had the maximum short-circuit current density and conversion efficiency compared to the other solar cells. This is due to the broader range of light absorption, which is also clearly evident in the UV-Vis absorption spectra and cyclic voltammetry curves.

Table 2: Current-Voltage characteristics of the fabricated natural DSSCS.

Solvent	I_{sc} (mA)	V_{oc} (mV)	FF	η%
without solvent	0.88	119	0.71	0.15
ethanol	1.04	250	0.75	0.35
acidified ethanol	1.29	360	0.80	0.79

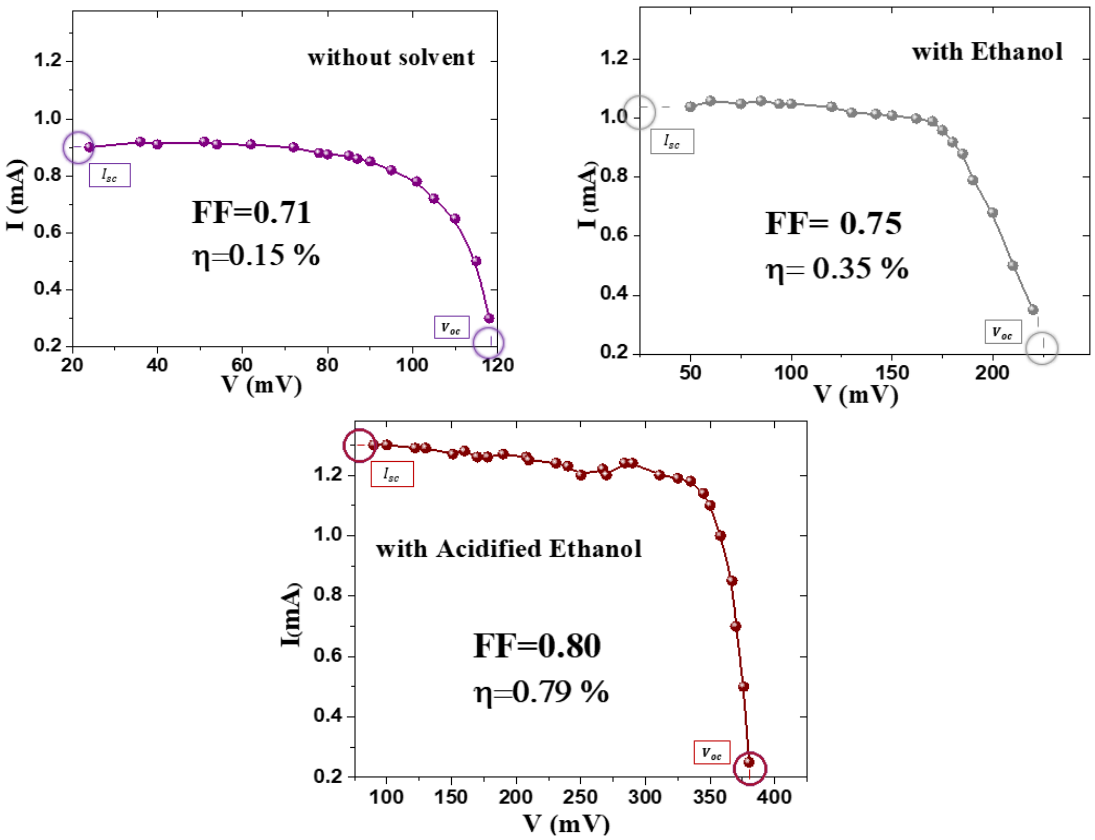

Figure 14: I-V characteristics of natural dye sensitized solar cells.

Conclusions:

The ZnO electrode was prepared using the sol-gel and dip-coating method with optimum experimental conditions for the solvent type, substrate withdrawal speed, and catalyst agent. The optimized film exhibited a nanoparticle size of about 48nm with a band gap energy of 3.26 eV. The values of E_{HOMO} and E_{LUMO} of the Shami berries extract were determined to be -5.2 eV and -3.5 eV, respectively. These values confirm the extent of alignment between the energy levels of the Shami berries extract and the energy gap value of ZnO. The efficiency of the dye sensitized solar cells varied from 0.15% to 0.79%. Natural dyes utilized as sensitizers for DSSCs represent a promising alternative to synthetic sensitizers due to their environmental friendly nature and low cost.

Data Availability

The data used to support the findings of this study are included within the article.

Conflicts of Interest

The authors declare that there are no conflicts of interest regarding the publication of this article.

References:

[1] S. Mohan, M. Vellakkat, A. Aravind, and Reka U, "Hydrothermal synthesis and characterization of Zinc Oxide nanoparticles of various shapes under different reaction conditions," *Nano Express*, vol. 1, no. 3, pp. 0300028-0300042, 2020.

[2] S. Bhatt, R. Shukla, C. Pathak, and S. Kumar, "Evaluation of performance constraints and structural optimization of a core-shell ZnO nanorod based eco-friendly perovskite solar cell," *Sol. Energy*, vol. 215, no. January, pp. 473–481, 2021, doi: 10.1016/j.solener.2020.12.069.

[3] L. Qin, F. J. Mawignon, M. Hussain, N. K. Ange, S. Lu, and M. Hafezi, "Economic Friendly

ZnO-Based UV Sensors Using Hydrothermal Growth : A Review," *Materials*, vol. 14, pp. 4083-4109, 2021.

[4] D. Kamaruzaman, N. Ahmad, and M. A. Rosly, "Piezoelectric energy harvesting based on ZnO : A review," *AIP Conference Proceedings* 2332, vol. 120002, pp. 1-5, 2021.

[5] A. Wibowo, A. Marsudi, I. Amal, M. B. Ananda, R. Stephanie, and L. Jaya, "ZnO nanostructured materials for emerging solar cell applications," *RSC Advances*, vol. 10, pp. 42838–42859, 2020, doi: 10.1039/d0ra07689a.

[6] M. T. Noman, N. Amor, M. Petru, A. Mahmood, and P. Kejzlar, "Photocatalytic Behaviour of Zinc Oxide Nanostructures on Surface Activation of Polymeric Fibres," *Polymers*, vol. 13, pp. 1227-1245, 2021.

[7] L. Zhu and W. Zeng, "Review of ZnO-based nanomaterials in gas sensors," *Solid State Ionics*, vol. 360, pp. 115544- 115566, 2017, doi: 10.1016/j.sna.2017.10.021.

[8] P. A. Luque-Morales , Lopez-peraza, Nava-Olivas, Amaya-Parra, Baez-Lopez, Orozco-Carmona, Garrafa-Galvez and Chinchillas-Chinchillas, "ZnO Semiconductor Nanoparticles and Their Application in Photocatalytic Degradation of Various Organic Dyes," *Materials*, vol. 14, pp. 7537-7555, 2021.

[9] C. Boon, L. Yong, and A. Wahab, "A review of ZnO nanoparticles as solar photocatalysts : Synthesis , mechanisms and applications," *Renew. Sustain. Energy Rev.*, vol. 81, pp. 536-551, 2018, doi: 10.1016/j.rser.2017.08.020.

[10] K. Yoo , W. Lee, K. Kang, I. Kim, D. Kang, D. Kyo Oh, M. Kim, H. Choi, K. Kim, J. Kim, I. Park and J. Ok, "Low-temperature large area fabrication of ZnO nanowires on flexible plastic substrates by solution processible metal seeded hydrothermal growth," *Nano Convergence*, vol. 7, pp. 24-34, 2020 doi: 10.1186/s40580-020-00235-6.

[11] N. Babayevska, L. Przysiecka, G. Nowaczyk, M. Jarek, M. Jarvekulg, T. Kangur, E. Janiszewska, S. Jurga and I. Iatsunskyi, "Fabrication of Gelatin-ZnO Nanofibers for Antibacterial Applications," *Materials*, vol. 14, pp. 103-115, 2021.

[12] A. Ahmed, A. Sabah, A. Naser and A. Munirah, " Enhancement of ZnO Nanorods Properties Using Modified Chemical Bath Deposition Method: Effect of Precursor Concentration," *Crystals*, vol. 10, pp. 386-400, 2020.

[13] H. Tseng, C. Wang, F. Wang, H. Liu, and C. Yang, "A Novel Synthesis of ZnO Nanoflower Arrays Using a Lift-Off Technique with Different Thicknesses of Al Sacrificial Layers on a Patterned Sapphire Substrate," *Nanomaterials*, vol. 12, pp. 612- 631, 2022.

[14] Cho. Junhee, H. Seongkwon, K. Hyun and Ch. seungjun, "Transparent ZnO Thin-Film Deposition by Spray pyrolysis for high-performance metal - oxide field - effect transistors," *Materials*, vol. 12, pp. 3423-3437, 2019.

[15] R. Yumiyama, D. Hyakutake, M. Hagiwara, E. Hosono, H. Matsuda, and S. Fujihara, "Chemical bath deposition of transparent ZnO films incorporated with erythrosine B molecules and their synergetic electro / photochromic properties," *Cryst Eng Comm*, vol. 16, pp. 14–21, 2020, doi: 10.1039/d0ce00167h.

[16] Z. Wang, *C.* Luo, W. Anwand, A.Wagner, M.Butterling, M.Azizar Rahman,M.Phillip, C That, M.Younas,Sh Su and F. Ling, "Vacancy cluster in ZnO films grown by pulsed laser deposition," *Scientific Reports*, vol. 9 , pp. 1–10, 2019, doi: 10.1038/s41598-019-40029-3.

[17] V. Kumar, R. Gupta, and A. Bansal, "Hydrothermal Growth of ZnO Nanorods for Use in Dye-Sensitized Solar Cells," *ACS Appl. Nano Mater*, vol. 4, pp. 6212-6222, 2021, doi: 10.1021/acsanm.1c01012.

[18] C. C. Substrates, I. Boukhoubza, E. Matei, A. Jorio, and M. Enculescu, "Electrochemical Deposition of ZnO Nanowires on CVD - graphene / copper substrates," *Nanomaterials*, vol. 12, pp. 2858- 2866, 2022.

[19] S. P. Singh, "Synthesis of Zinc Oxide Nanoparticle by Sol-Gel Method and Study its Characterization," *International Journal for Research in Applied Science and Engineering Technology*, vol. 8, pp. 1625-1627, 2020, doi: 10.22214/ijraset.2020.4265.

[20] K. Davis, R. Yarbrough, M. Froeschle, and J. White, " Band gap engineered zinc oxide nanostructures via a sol – gel synthesis of solvent driven shape- controlled crystal growth," *RSC Advances*, vol. 9, pp. 14638–14648, 2019, doi: 10.1039/c9ra02091h.

[21] C. C. Vidyasagar and B. M. Mun, "Recent Advances in Synthesis and Properties of Hybrid Halide Perovskites for Photovoltaics," *Nano-Micro Lett*, vol. 10, pp. 68-102, 2018.

[22] K. Sharma, V. Sharma, and S. S. Sharma, "Dye-Sensitized Solar Cells : Fundamentals and Current Status," *Nanoscale Research Letters,* vol. 13, pp. 381-427, 2018.

[23] B. Bekele, L. T. Jule, A. Saka, "The effects of annealing temperature on size, shape, structure and optical properties of synthesized zinc oxide nanoparticles by sol-gel methods," *Digest Journal of Nanomaterials and Biostructures,* vol. 16, p. 471 - 478, 2021

[24] . رسالة ماجستير، قسم الفيزياء، "دراسة إمكانية تحضير خلايا شمسية صباغية باستخدام بنى نانوية من أوكسيد الزنك"عامر قاعدة بيانات مديرية البحث العلمي ، 2019كلية العلوم، جامعة دمشق، سورية، http://damascusunivertsity.edu.sy\srd.

[25] A. AL-Zahrani, Z. Zainal, Z. Talib, J. Ngee, L. Fudzi, A. Holi and M. Sarif, "Effect of Hydrothermal Growth Temperature and Time on Physical Properties and Photoanode Performance of ZnO Nanorods," *International Journal of Nanoelectronics and Materials,* vol. 13, pp. 381-400, 2020.

[26] A. M. Alsaad, Q. M. Al-bataineh, A. A. Ahmad, Z. Albataineh, and A. Telfah, "Optical band gap and refractive index dispersion parameters of boron-doped ZnO thin films : A novel derived mathematical model from the experimental transmission spectra," *Opt. - Int. J. Light Electron Opt.*, vol. 211, pp. 164641- 164654, 2020, doi: 10.1016/j.ijleo.2020.164641.

[27] Z. Arifin, S. Soeparman, D. Widhiyanuriyawan, A. Setyaji, "Improving stability of chlorophyll as natural dye for dye sensitized solar cells," *Jurnal Teknlogi*, vol. 80, pp. 27-33, 2018.

[28] W. Almaz, H. Salleh, and M. Zalani, "Optik Low cost dye-sensitized solar cells based on zinc oxide and natural anthocyanin dye from Ardisia elliptica fruits," *Optik,* vol. 172, pp. 28–34, 2018, doi: 10.1016/j.ijleo.2018.06.041.

[29] O. I. Francis and A. Ikenna, "Review of Dye-Sensitized Solar Cell (DSSCs) Development," *Advances in OptoElectronics,* vol. 13, pp. 496–509, 2021.

[30] C. Prouskas, A. Mourkas, G. Zois, E. Lidorikis, and P. Patsalas, "A New Type of Architecture of Dye-Sensitized Solar Cells as an Alternative Pathway to Outdoor Photovoltaics," *Energies,* vol. 15, pp. 2486-2500, 2022.